
This is an electronic reprint of the original article.
This reprint may differ from the original in pagination and typographic detail.

Ihalainen, Mika; Kortelainen, Miika; Mesceriakovas, Arunas; Karhunen, Tommi;
Mesceriakove, Sara Maaria; Lindberg, Daniel; Leskinen, Jari T.T.; Kankaanpää, Timo;
Jokiniemi, Jorma; Lähde, Anna

Synthesis of solid NMC622 particles by spray drying, post-annealing and lithiation

Published in:
Advanced Powder Technology

DOI:
[10.1016/j.appt.2023.104187](https://doi.org/10.1016/j.appt.2023.104187)

Published: 01/10/2023

Document Version
Publisher's PDF, also known as Version of record

Published under the following license:
CC BY

Please cite the original version:
Ihalainen, M., Kortelainen, M., Mesceriakovas, A., Karhunen, T., Mesceriakove, S. M., Lindberg, D., Leskinen, J. T. T., Kankaanpää, T., Jokiniemi, J., & Lähde, A. (2023). Synthesis of solid NMC622 particles by spray drying, post-annealing and lithiation. *Advanced Powder Technology*, 34(10), Article 104187.
<https://doi.org/10.1016/j.appt.2023.104187>

This material is protected by copyright and other intellectual property rights, and duplication or sale of all or part of any of the repository collections is not permitted, except that material may be duplicated by you for your research use or educational purposes in electronic or print form. You must obtain permission for any other use. Electronic or print copies may not be offered, whether for sale or otherwise to anyone who is not an authorised user.



Original Research Paper

Synthesis of solid NMC622 particles by spray drying, post-annealing and lithiation



Mika Ihalainen^{a,*}, Miika Kortelainen^a, Arunas Meserikovas^a, Tommi Karhunen^a, Sara-Maaria Meserikove^a, Daniel Lindberg^b, Jari T.T. Leskinen^c, Timo Kankaanpää^d, Jorma Jokiniemi^a, Anna Lähde^a

^a Fine Particle and Aerosol Technology Laboratory, Department of Environmental and Biological Sciences, University of Eastern Finland, 70210 Kuopio, Finland

^b Aalto University, School of Chemical Engineering, Department of Chemical and Metallurgical Engineering, P.O. Box 16100, Aalto 00076, Finland

^c SIB Labs, University of Eastern Finland, 70210 Kuopio, Finland

^d Umicore Finland Oy, 67100 Kokkola, Finland

ARTICLE INFO

Article history:

Received 24 April 2023

Received in revised form 7 July 2023

Accepted 26 July 2023

Available online 11 August 2023

Keywords:

Spray drying

Non-hollow particles

NMC622 cathode material

NMC622 oxide lithiation

ABSTRACT

Layered lithium-nickel-manganese-cobalt oxide (NMC) cathode materials are widely used in Li-ion batteries that require high energy densities, such as those used in plug-in hybrid electric vehicles (PHEVs) and electric vehicles (EVs). Here we studied the synthesis of NMC622 particles by spray pyrolysis, which is a simple one-step process for production of spherical particles. However, synthesising NMC powder using spray pyrolysis has a tendency to produce hollow NMC particles. To gain insight into the mechanism behind the formation of the hollow particles, one dimensional numerical simulation of the physical and chemical phenomena taking place during spray drying were carried out. The effects of several process parameters, including drying air temperature, drying air mass flow rate, and liquid feed mass flow rate, on the evaporation and particle formation process were studied. The increased evaporation rate at higher temperatures was found to result in crust formation on the droplet surface during the particle formation, and thus, in lower solid volume fractions in the dried particles. However, by optimizing the process parameters production of solid NMC622 sulphate particles by spray drying was achieved. The produced NMC622 sulphate particles were then oxidised and lithiated in air at 850 °C via the conventional thermal treatment process. Four lithium precursors, LiOH, Li₂CO₃, Li₂SO₄ and LiNO₃, were tested for the lithiation of the oxidized NMC particles. The degree of lithiation and the crystalline phase of the powders were determined using ICP-OES and XRD, respectively.

© 2023 The Society of Powder Technology Japan. Published by Elsevier B.V. and The Society of Powder Technology Japan. This is an open access article under the CC BY license (<http://creativecommons.org/licenses/by/4.0/>).

1. Introduction

Layered lithium-nickel-manganese-cobalt oxide (NMC) cathode materials are widely used in Li-ion batteries that require high energy densities, such as those used in plug-in hybrid electric vehicles (PHEVs) and electric vehicles (EVs). Conventional synthesis methods such as co-precipitation [1,2] and solid-state processes [3] are currently used in industry. However, these are complex processes, particularly in terms of their physical and chemical phenomena. For co-precipitation, several single-unit processes are sometimes required, as well as long reaction times. Additionally, by-products are formed from the chemicals used in the co-precipitation synthesis processes. A cost analysis of NMC syn-

thesised by co-precipitation [4] showed the importance of labour, energy consumption, and time requirements on the overall costs of NMC production.

To simplify the synthesis of NMC, the use of one-stage processes such as spray pyrolysis [5,6], flame-assisted spray pyrolysis and spray roasting [7,8] has been reported recently. The one-stage processes such as spray pyrolysis and flame-assisted pyrolysis methods can potentially reduce around 17 % of the costs compared to the conventional costs [9]. Typically, metal nitrates have been used as precursors in spray pyrolysis, with few exceptions including the studies of metal chlorides by Li et al. [10], for example. However, metal nitrates are typically more expensive than sulphates. In addition, most metal refining processes are sulphate-based, and thus sulphates are more readily available.

Both spray drying and pyrolysis are a widely used process in the pharmaceutical and food industries. However, the morphology of

* Corresponding author.

E-mail address: mika.ihalainen@uef.fi (M. Ihalainen).

the final product is a problem in one-step spray pyrolysis and roasting. For example, in spray pyrolysis, hollow particles are usually formed [5]. In some studies, researchers have attempted to identify the process conditions for obtaining solid dense or hollow particles [11]. These studies were conducted using very broad process conditions and in different laboratories, and thus no comprehensive understanding of the effects on the final particle morphology could be obtained.

In other studies, additional processing of hollow particles [12] was carried out to obtain denser NMC particles after spray pyrolysis. These studies showed that by using additional processing steps such as ball milling and then making a water solution of the milled particles and subjecting them to spray pyrolysis a second time, one can obtain NMC particles with quite good electrochemical properties after calcination. In [13,14], chemical additives were used in the spray pyrolysis of NMC cathode materials. These studies showed that chemical additives can prevent hollow particle formation and that doping with metals can improve the electrochemical performance of the material. However, the additives add complexity to the precursor solutions used for the spray drying and/or pyrolysis, and can leave traces of impurities to the produced particles, if they are not removed completely during the solid particle formation. In another study, [15] recovered NMC cathode active materials were synthesised by spray pyrolysis of spent cathode scraps using organic solvents. After leaching, the recovered metals were converted into lithium acetate, nickel acetate, cobalt acetate, and manganese acetate for spray pyrolysis. However, the conversion process is also relatively complex and thus, expensive. In addition, due to the small droplet size, i.e., nano-sized, used in this spray pyrolysis system, the yield of the final product was very low.

In this study, spray drying of aqueous NMC 622 sulphate solution was carried out at mild temperatures for the synthesis of solid NMC 622 particles. A systematic study on the particle formation, morphology and composition was carried out. The process parameters affecting the solid particle formation in the spray drying process were optimized with the numerical simulations. Due to the low reaction temperatures applied to ensure solid particle formation, a post-oxidation and lithiation was carried out to obtain final lithiated NMC 622 particles.

2. Methods

2.1. Precursors

A 2 M metal sulphate–water solution was used as the precursor for NMC622 particle production. For lithiation, the solubility of four solid lithium compounds in the NMC622 sulphate solution was studied. The lithium compounds used were Li_2SO_4 , LiOH , LiNO_3 , and Li_2CO_3 . NMC622 was mixed with Li at a 1:1 M ratio. The solubility of the lithium compounds was studied by mixing the required mass of the Li compound into a 10-mL NMC solution at room temperature using a magnetic stirrer.

2.2. Numerical simulation of particle formation in spray drying

The evaporation process of the water solution droplets was modelled in pipe geometry using a one-dimensional (1D) modelling approach. The 1D simulation was chosen over the 3D because the code is easier to implement, and the computational cost is significantly lower than that in 3D. The obvious restriction of the 1D simulation is that the other two dimensions were not simulated, and thus the phenomena occurring in those dimensions were disregarded. An important process to which this restriction applies was the mixing of the sprayed droplets with the drying air at the very beginning of the geometry. Mixing plays an impor-

tant role, particularly in high-temperature cases where evaporation occurs rapidly. Mixing slows evaporation by restricting the heat available for the evaporation process. In addition, the evaporation process may be limited to the mixing zone by saturated water concentration. In a real case, some of the droplets mix with the drying air faster than other droplets. This produces heterogeneity in the evaporation process and dried-particle outcomes.

To capture the evaporation process, the heat transfer between the droplets, gas phase, and walls were considered, as well as the mass transfer from the droplet to the gas phase (Fig. 1). The evaporation process was modelled until crust formation occurred, that is, until the critical concentration for crust formation was reached. At this point, an estimation was made whether the particles were likely to form hollow or solid particles. The processes occurring after crust formation, such as physical transformation of the crust, were not simulated, nor was the heat transfer within the droplet considered.

The evaporation part of the model follows the model reported by Xion and Kodas [16] and is briefly described here. The change in droplet size (i.e., droplet-size time derivative dd_p/dt) owing to the evaporation process is

$$\frac{dd_p}{dt} = \frac{4D_v m_1}{\rho_p d_p} (n - n_s), \quad (1)$$

where D_v is the vapour diffusion coefficient in air, m_1 is the mass of the water molecule, d_p is the droplet diameter, ρ_p is the density of the droplet, and n and n_s are the vapour concentration in air and droplet surface, respectively.

The evaporated water concentration is then transferred to the gas phase. The water vapour concentration at the surface of the droplet is defined as

$$n_s = \frac{p_{sat}}{k_B T_s}, \quad (2)$$

where T_s is the temperature of the droplet surface, k_B is the Boltzmann constant, and p_{sat} is the saturation vapour pressure at the droplet surface. This equilibrium vapour pressure p_{sat}^0 is lowered by the presence of the solute, and this reduction may be expressed with the help of water activity a_a as

$$p_{sat}(T_s) = a_a p_{sat}^0(T_s). \quad (3)$$

The droplet surface temperature T_s is affected by the latent heat of evaporation and the heat transfer between the surrounding gas phase and the droplet.

$$\frac{dT_s}{dt} = \frac{1}{C_p d_p} \left[3H_L \frac{dd_p}{dt} + \frac{6h_s}{\rho_p} (T - T_s) \right], \quad (4)$$

where H_L is the latent heat of water evaporation, h_s is the heat-transfer coefficient around the droplet, T is the gas temperature, and C_p is the heat capacity of the droplet.

The temperature of the gas is affected by both heat transfer to the droplets and heat transfer from the walls. This can be expressed as

$$\frac{dT}{dx} = \frac{1}{F_a C_{pa}} \left[-\pi^2 R_t^2 D_p^2 N_\infty n_s (T - T_s) + 2\pi R_t h_w (T_w - T) \right], \quad (5)$$

where C_{pa} is the heat capacity of wet air, h_w is the heat-transfer coefficient at the reactor wall, T_w is the wall temperature, F_a is the air molar flow rate, R_t is the wall radius, and N_∞ is the droplet number concentration. A binary solution was thus considered.

Evaporation of the solvent increases the concentration of the non-evaporating precursor material on the surface of the droplet increases, that is, a concentration gradient is formed within the droplet. This concentration gradient induces diffusion flux of the precursor material toward the centre of the droplet. In this study,

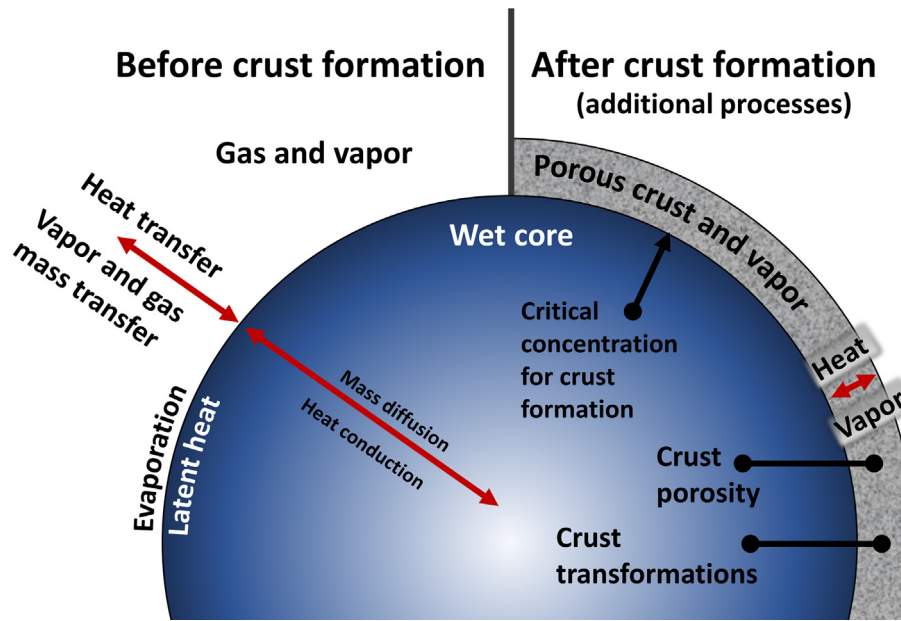


Fig. 1. Scheme of different phenomena taking place in the droplet during the spray drying process.

the changes in diffusion-induced concentration inside a droplet were modelled assuming spherical symmetry, that is, the concentration varied only in the radial direction. Fick's second law for diffusion in spherically symmetric cases can be written as

$$\frac{\partial C}{\partial t} = \frac{D}{r^2} \frac{\partial}{\partial r} \left(r^2 \frac{\partial C}{\partial r} \right), \quad (6)$$

where r is the radial coordinate, t is the time, D is the diffusion coefficient, and C is the concentration. This equation was coupled with the evaporation model and solved numerically for each time step. Another process affecting the mixing and concentration gradient within the droplet is convection; however, this process was not considered here.

Because the evaporation process increases the concentration of the precursor material at the surface of the droplet, the critical concentration triggering crust formation at the surface of the droplet is reached. The critical concentration required for crust formation was estimated for Ni^{2+} , Mn^{2+} , and Co^{2+} with the solubility product K_{sp} [17].

$$S = \frac{[A][\text{SO}_4^{-2}]}{K_{sp}} \quad (7)$$

where S is the supersaturation ratio, and A may be Ni^{2+} , Mn^{2+} , or Co^{2+} . Any of the metal ions (Ni^{2+} , Mn^{2+} , or Co^{2+}) may trigger crustal formation. Slight supersaturation was assumed in the simulations ($S = 1.1$). The processes occurring after crust formation, such as crust shrinkage or explosion, were not modelled here. The void inside the particles after crust formation was estimated as follows:

$$\text{solid volume percentage} = \frac{V_{m_{\text{initial}} - \rho_{\text{crit}, S=1}}}{V_{\text{dried particle}}} \quad (8)$$

where $\rho_{\text{crit}, S=1}$ denotes the solute density at $S = 1$. The particle is present throughout the solid if $S \geq 1$ over the entire particle as the crust forms. The parameter $V_{\text{dried particle}}$ is the volume of the particle at the moment the crust forms and the simulation ends, and the minor parameter m_{initial} is the precursor mass content of the droplet.

2.3. Spray drying

A modified Pilotech spray dryer (YC-015) was used in this study. In this spray dryer, the droplets were first atomised from the precursor solution in the spray nozzle with the help of pressurised air. The droplets were then dried by mixing them with 300–600 L/min of air at normal temperature and pressure (NTP, 20 °C, 1 atm) in the drying chamber. The dried particles were collected using a cyclone downstream of the drying chamber (Fig. 2). In these experiments, the spray dryer was modified so that the cyclone was replaced by a virtual impactor with a D50 cut-off size of 0.8–1.3 μm depending on the total flow rate through the virtual impactor and filter combination for particle collection purposes. Thus, the width of the particle-size distribution was narrower and the gas flow rate to the filter collecting the particles was significantly decreased. The gas flow to the filter was approximately 5 L/min at NTP.

2.4. Heat treatment of spray-dried NMC622 sulphate particles

Spray-dried NMC622 sulphate particles were heat treated in a muffle furnace at 600, 700, 800, and 900 °C for 30 min in air. The change in particle morphology as a function of temperature was observed using scanning electron microscopy (SEM), and the tapped density, colour, and NMC622 dry sulphate powder oxidation were observed using thermogravimetric analysis (TGA) and inductively coupled plasma-optical emission spectrometry (ICP-OES).

2.5. Lithiation and oxidation

Oxidation of NMC622 powder was performed by heating the sample in a muffle furnace at 850 °C for 3 h in an oxidising atmosphere. After oxidation, lithium was mixed with the oxidised NMC at an excess molar ratio of 5%. Four lithium compounds were used: Li_2SO_4 , LiOH , Li_2CO_3 , and LiNO_3 . Lithiation was performed in the muffle furnace at 850 °C for 16 h in air oxidising atmosphere. After lithiation, excess lithium was washed from the samples with 150 mL of ion exchanged water per 5 g of lithiated NMC. The slurry was mixed for 20 min using a magnetic stirrer and then filtered

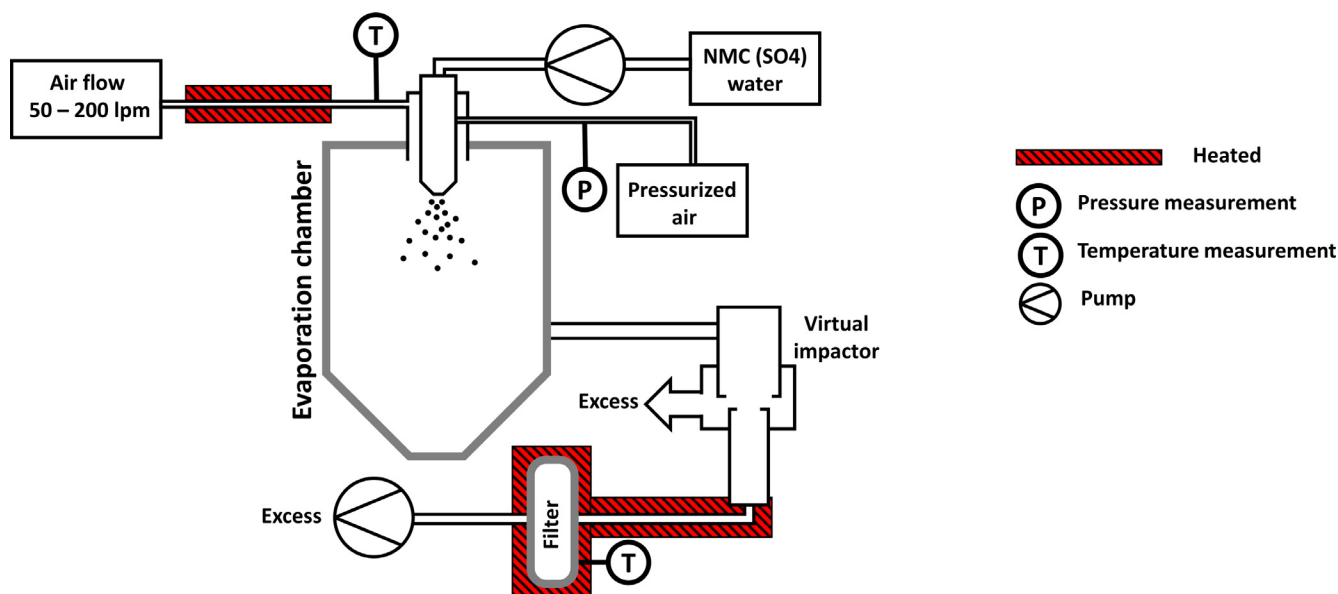


Fig. 2. Operating principles of the modified spray dryer.

using a membrane filter (Whatman, Regenerated cellulose RC55). Water removal was done by heating samples at 190 °C for 16 h.

2.6. Characterisation

TGA analysis (Q50, TA instruments, USA) of the initial NMC sulphate solution and spray-dried powder was performed in air to obtain the weight percentage of the different components in the samples. Before the analysis, water was evaporated to form solid NMC sulphate but not to complete dryness. The sample was then placed in the TGA system, equilibrated at 50 °C for 15 min, and then heated to 1000 °C at a rate of 10 °C/min.

For the samples where lithium compounds were added to the NMC622 dry sulphate precursor, the mixture was first equilibrated at 30 °C. They were then heated to 400 °C at a rate of 10 °C/min, followed by an isothermal period of 15 min. After this, the temperature was rapidly increased to 850 °C with an isothermal time of 120 min at this temperature. When using lithium sulphate for lithiation, we used an additional jump from 850 °C to 900 °C with a 25-min isotherm time and then a jump to 950 °C because the reactions were not complete at the lower temperatures.

X-ray diffraction (XRD) analysis was performed on a Bruker AXS D8 Advance system (Cu K α source, 40 kV, 40 mA) and analysed using Topas 3 software. The diffraction was measured between 2 θ angles of 10° and 80° with a step size of 0.06°. The crystal sizes, d_{XRD} , were calculated using the fundamental parameter approach and the Rietveld method.

The tapped density was determined using a JZ-7 tap density analyser, according to ISO 3953:2011 standard. A cylinder with a volume of 25 mL and a scale readable to 1 mL was used as the sample container. The tapping height of the analyser was 3 ± 0.2 mm. Tapping was performed in steps of approximately 1000 taps until no reduction in volume was observed. After tapping, the samples were weighed with an accuracy of 0.1 mg.

Morphological and structural analyses were performed using field-emission scanning electron microscopy (FE-SEM; Zeiss Sigma HDVP, Carl Zeiss NTS, Cambridge, UK). The sample powders were placed on double-sided carbon tape mounted on standard half-inch aluminium stubs. The geometric mean diameter of the primary particles and the geometric standard deviation (GSD) of the size data was determined from a large sample population of parti-

cles ($N > 300$) imaged with SEM. For standard SEM analysis, the ion beam slope-cutting technique was used to cut the particles and reveal the interior of the dried particles. For ion milling, the produced humidity-sealing cyanoacrylate fast-glue polymer and attached to aluminium foil. The foil was then fixed to the sample stub. The sample stub contained a tungsten mask that partially separated the sample from the ion beam to produce a cross section of the material to be studied. Cross sectioning was performed using a Leica EM RES102 ion beam milling system (Leica Microsystems GmbH, Vienna, Austria). An argon ion beam operating at 6 kV was used for slope cutting ($\alpha = 3^\circ$) of the sample protruding from the tungsten mask.

Elemental analysis of the oxidised NMC622 and lithiated NMC622 samples was performed using ICP-OES. Sodium peroxide fusion (Method 721P), used for the sample digestion for ICP-OES analysis, is a total digestion method for major elements in refractory ore minerals, high-grade base metals and iron ores, and concentrates. Thus, the prepared pulp sample (0.2 g) was fused with sodium peroxide flux at 720 °C for 20–25 min. The cooled sample was dissolved in 50 mL of 4 M HCl. The final solution was diluted with 20% aqua regia prior to ICP-OES analysis.

3. Results

3.1. Thermal behaviour of sulphate solution and dry powder

We carried out laboratory-scale studies using TGA and thermodynamic equilibrium calculations (see [Supplemental Information](#)). In this study, we used an industrial-grade NMC622 sulphate solution with a total metal content of 2 M in water.

The TGA results are shown in [Fig. 3](#). The TGA data was normalised with 100 a.u., corresponding to the final mass at 900 °C. This was performed for easy comparison of the results. The theoretical mass loss owing to MSO_4 dissociation ($\text{MSO}_4 \rightarrow \text{MO}_2 + \text{SO}_2$) for the dry NMC622 sulphate was 49.7%. The experimentally observed mass losses between 500 °C and 900 °C were 49.6% and 45.5% for the 2 M NMC622 sulphate solution and spray-dried sulphate powder, respectively, values that corresponded well with the theoretical values. The observed mass loss before 500 °C was attributed to water evaporation for both samples.

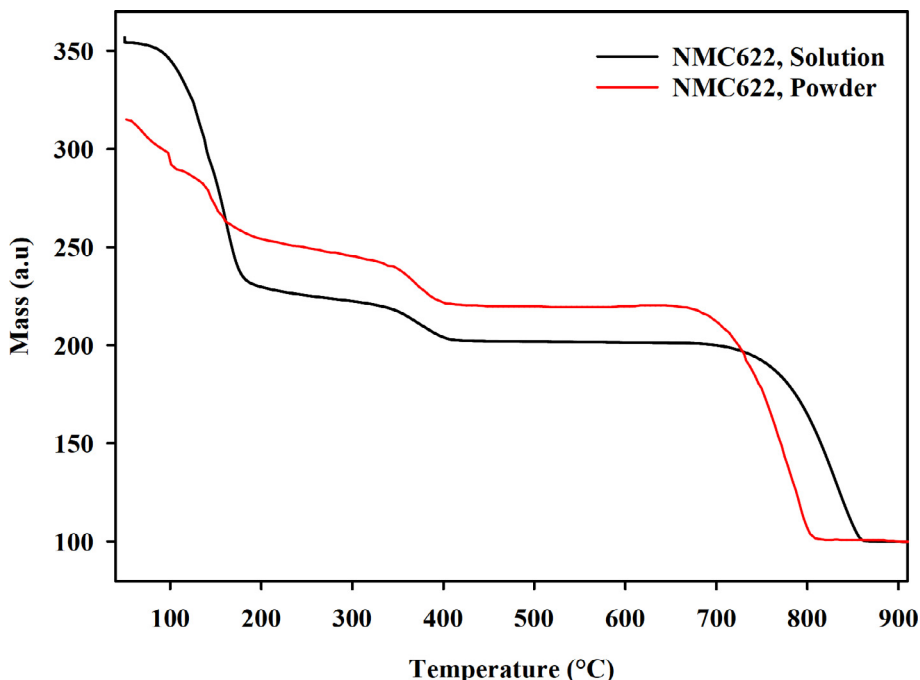


Fig. 3. Comparison of TGA results from spray- dried NMC622 sulphate powder and pre-dried NMC622 sulphate solution at heating rate of 10 °C/min. The data of the y-axis is fitted providing relative changes of the masses to enable better comparison of the values.

3.2. Spray drying

3.2.1. Simulation results of particle formation in spray drying

The evaporation of NMC622 sulphate–water solution droplets was numerically simulated in 1D, and the results are presented in Fig. 4. The evaporation process was carried out by varying the system parameters of drying air temperature, drying air mass flow rate, and liquid feed mass flow rate. The droplet-size distribution was assumed to have a geometric mean diameter (GMD) of 50 µm and a geometric standard deviation (GSD) of 1.7. Particles within 2.5 GSD from the GMD were considered.

According to the simulations, the evaporation rate increased with increasing temperature as expected, resulting in lower solid volume percentages of the dried particles, that is, more hollow particles. Thus, by decreasing the drying air temperature, particles with higher solid volume percentages were formed.

In addition to temperature, another parameter that reduced the evaporation rate according to the calculations was the air mass flow-to-liquid mass flow ratio. At low ratios, the water vapour content of the air became an evaporation-limiting factor as the relative humidity (RH) increased. This induced slower evaporation rates and thus higher solid volume percentages of the dried particles, that is, denser particles. However, these conditions may also lead

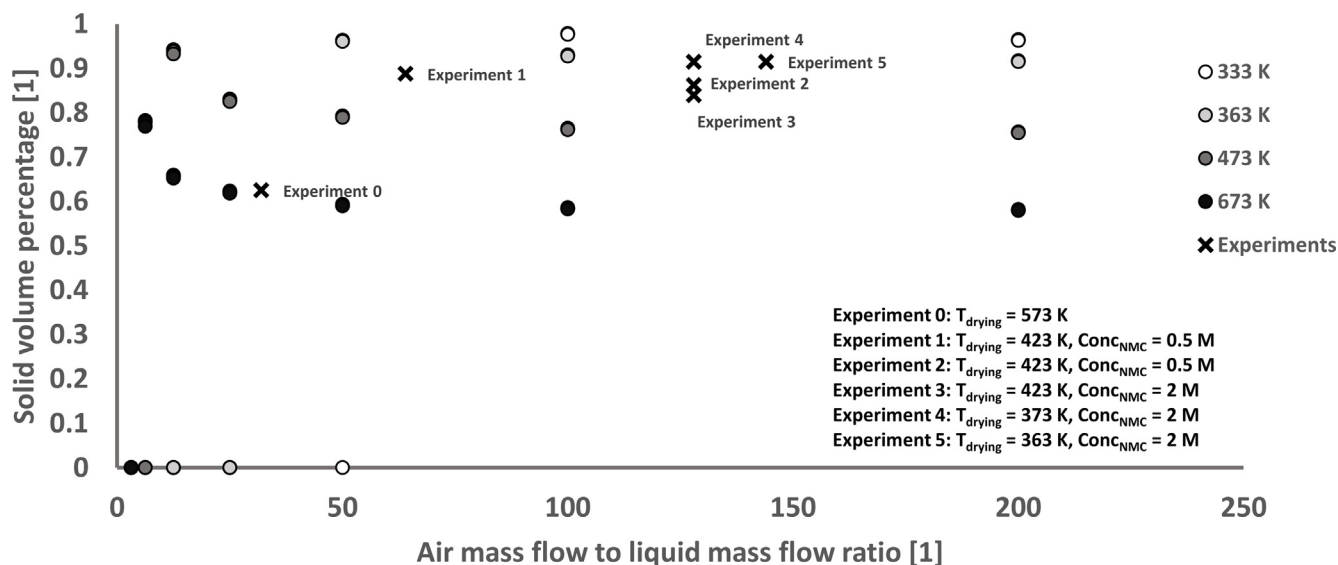


Fig. 4. Simulated solid volume percentages (Eq. (8)) of the dried particles (indicated as spheres) as a function of air mass flow-to-liquid mass flow ratio. Simulations at different drying air temperatures between 333 K and 673 K are shown. The simulations were also carried out at the conditions of the experiments 0–5 (Table 1) and these results are shown with 'x' marker.

to formation of particles that are not dry enough to form any crust because of water saturation in the gas phase or lack of sufficient residence time in the dryer. In the case of high air mass flow-to-liquid mass flow rate ratios, the solid volume percentages of the dried particles seemed independent of the ratio itself. The value where the solid volume percentage became independent of the flow ratios depended on temperature because the saturation vapour pressure depends strongly on temperature. In addition, the particle size strongly affected the time required for evaporation; however, it had only a minor effect on the solid volume percentage value of the dried particles.

3.2.2. Spray drying of NMC622 sulphate–water solution

The synthesis parameters were optimized based on the obtained simulation results. The parameters that could be varied in our spray-drying system were (1) atomiser pressure, which directly affects the droplet size (with higher pressure, smaller dro-

plets were obtained), (2) temperature of the drying air, (3) liquid feed rate, (4) drying air flow rate, and (5) precursor concentration. The metal (Ni + Mn + Co) concentration in the metal sulphate NMC622 water solution was 2 M.

Several experiments were performed to determine the optimal parameters for spray drying to obtain solid particles. The effect of the parameters on the particles was initially evaluated visually from the SEM images with the help of the evaporation model. The optimal parameters were then confirmed by observing the interior of the ion-milled particles. The varied parameters are presented in Table 1, and the corresponding SEM images of the particles produced in various experiments are shown in Figs. 5 and 6.

Fig. 4 shows the drying simulations conducted using the same parameters as those described in the experimental section. The simulations showed that the particles were very likely to be hollow because the evaporation parameters were 'unoptimised'. As the temperature was decreased to 90 °C and the air mass flow-to-

Table 1

Parameters of the spray drying experiments. The filter flow rate was 5 L min⁻¹ for all experiments.

	Experiment	Intermediate results	Air to liquid mass ratio	Drying temperature (°C)	Precursor feed rate (ml min ⁻¹)	NMC (metal) concentration (M)	Total gas flow (l min ⁻¹)	Atomizer pressure (bar)
Initial experiment	Experiment 0		32	300				
	Experiment 3	Fig. 5 (g – i)	128	150	3.75	2.0	400	3
	Experiment 4	Fig. 5 (j – l)	128	100	3.75	2.0	400	3
Precursor feed rate	Experiment 2	Fig. 5 (d – f)	128	150	3.75	0.5	400	3
	Experiment 1	Fig. 5 (a – c)	64	150	7.5	0.5	400	3
NMC concentration	Experiment 2	Fig. 5 (d – f)	128	150	3.75	0.5	400	3
	Experiment 3	Fig. 5 (g – i)	128	150	3.75	2.0	400	3
Final results	Experiment 5	Fig. 6	144	90	1.5	2.0	180	5

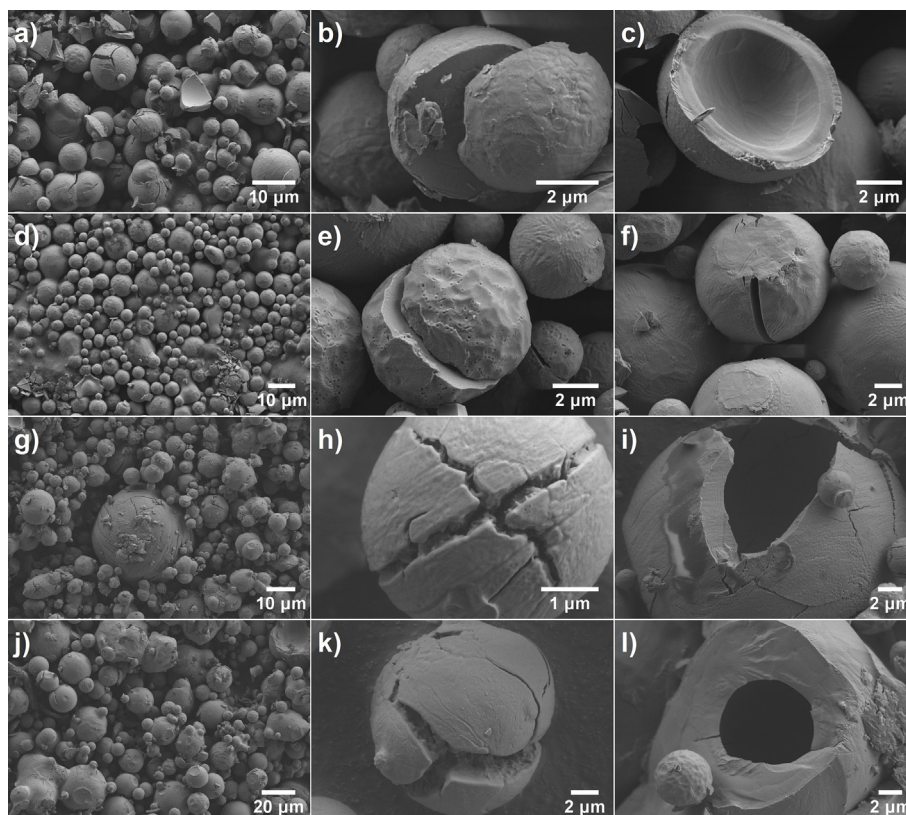


Fig. 5. EM micrographs of particles obtained with parameters specified in Table 1 for: (a–c) Experiment 1, (d–f) Experiment 2, (g–i) Experiment 3, and (j–l) Experiment 4.

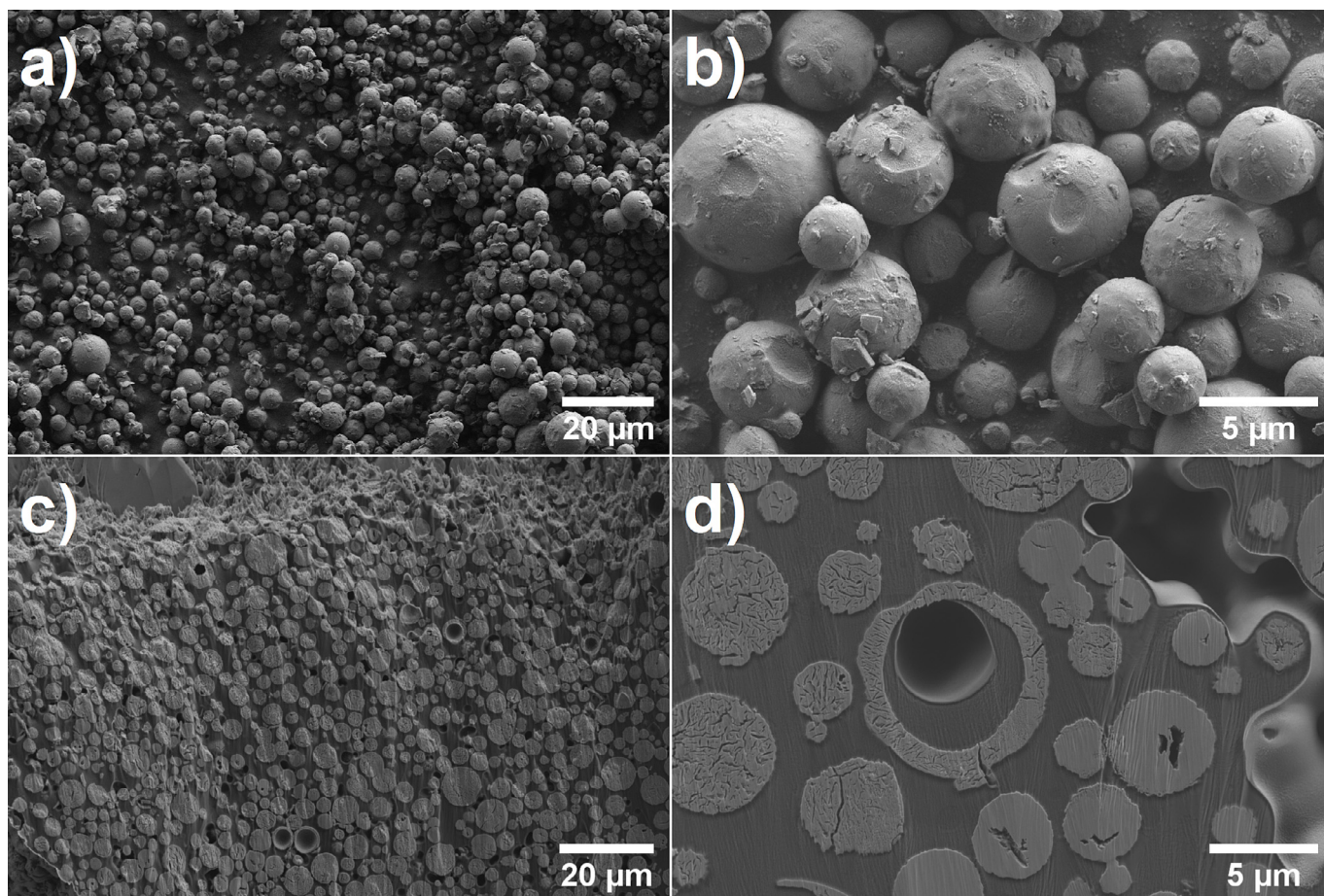


Fig. 6. (a) and (b) Spray dried NMC622 sulphate particles using optimised parameters (Experiment 5) as presented in Table 1; (c) and (d) Cross sections of ion-milled spray dried NMC622 particles.

liquid mass flow ratio increased above 100 to the 'optimised' settings, the solid volume percentages increased close to unity. This result is consistent with the experimental data.

3.3. SEM analysis of spray-dried particles

The initial parameters for *Experiment 0* (Table 1) clearly produced hollow particles with thin walls and collapsed structures (Fig. S8). This was because the evaporation rate was too fast, mainly owing to the high (300 °C) evaporation temperature. The evaporation model supports this as it gives a low solid volume percentage owing to the high evaporation temperature. Because of the initial extremely hollow particles, the evaporation temperature was reduced for the remainder of the experiments.

The drying temperature was further studied at 150 °C and 100 °C (Table 1, Experiments 3 and 4, respectively). Lowering the drying temperature allowed for slower evaporation, which was thought to impede the formation of hollow particles. The results (Fig. 5g and 5j) showed similar particles, some of which showed a collapsed structure (Fig. 5k), whereas other particles displayed a thicker interior wall (Fig. 5i, l). The evaporation model also showed that the solid volume percentage should increase as the temperature decreased from 150 °C to 100 °C. Overall, these particles did not show similar thin-walled and fragile behaviours as the particles in *Experiment 0*. This was mainly owing to the lower evaporation temperature.

Next, the precursor feed rate was doubled from 3.75 mL min⁻¹ (*Experiment 2*) to 7.5 mL min⁻¹ (*Experiment 1*). Fig. 5d–f show the NMC622 particles spray dried with the 3.75 mL min⁻¹ precursor

flow rate, and Fig. 5a–c show those with the 7.5 mL min⁻¹ precursor flow rate. The particle size was larger with a higher feed rate (SEM, N = 300, median $D_p = 4.9 \mu\text{m}$) than with a lower feed rate (SEM, N = 300, median $D_p = 4 \mu\text{m}$), which is likely owing to the higher droplet size produced in the atomiser with the higher liquid flow rate. The evaporation model showed that the low air mass-to-liquid mass flow ratio (i.e., higher liquid feed rate) in *Experiment 1* may have started to restrict the evaporation rate owing to the high RH of the water vapour. This should increase the solid volume percentage but it creates a risk of incomplete evaporation.

Following this, we increased the NMC (metal) concentration in the solution from 0.5 M (*Experiment 2*) to 2.0 M (*Experiment 3*). The particles had similar sphericity in both cases, and agglomeration was observed (Fig. 5g). In addition, some of these particles were larger than those observed previously, which was mainly owing to the increased solute concentration and agglomerate formation. The evaporation model showed that the solid volume percentage had only a minor dependency on the NMC metal concentration between *Experiments 2* and 3.

Experiment 4 yielded the most promising results based on the evaporation model and SEM images. Thus, for the final parameters, it was decided to further decrease the drying temperature, precursor feed rate, and total gas flow rate (Table 1, *Experiment 5*). In this case, the evaporation slowed even further while increasing the residence time and maintaining a high air mass flow-to-liquid mass flow ratio. As seen in Fig. 6, this yielded sphericity similar to that shown in earlier experiments and non-hollow particles. The particles were mostly present as single spherical particles. The size dis-

tribution (Fig. 7) of the particles was calculated from Fig. 6a, and the geometric mean diameter was estimated to be 3.3 μm with the geometric standard deviation of the size data set of $\text{GSD} = 1.44$. To assess the interior of the particles, ion milling was carried out, and the cross sections were imaged using SEM (Fig. 6c, d). The spray-dried particles had a solid interior, with only approximately 1% (counted from Fig. 6c, $N = 520$) of the particles showing a hollow interior.

3.4. Heat treatment and oxidation of dry NMC622 sulphate particles

The NMC622 sulphate powder produced with optimal parameters (Experiment 5) was heat treated in steps of 100 $^{\circ}\text{C}$ until 900 $^{\circ}\text{C}$ was reached. The holding time for each step was 30 min. The tapped

density of the powders, which is affected by the cation mixing and particle morphology, was measured after each increment. It was found that the tapped density increased from approximately 1 to 1.6 g cm^{-3} at 700–800 $^{\circ}\text{C}$ (owing to oxidation). It then slightly decreased when heated to 900 $^{\circ}\text{C}$ (owing to sintering and crystal growth) (Fig. 8). For comparison, similar studies were carried out by Lengyel et al. [5], and the highest tapped density obtained in that study was 0.86 g cm^{-3} after heating the spray-pyrolysed sample for 2 h in air at 900 $^{\circ}\text{C}$. Their median particle diameter was approximately 1.5 μm as measured by an electrical low-pressure impactor (ELPI), whereas our median particle diameter was 3.2 μm as determined from the SEM images ($n_{\text{particle}} = 360$) shown in Fig. 6.

Fig. 9 shows the heat-treated NMC622 sulphate particles at 600, 700, 800, and 900 $^{\circ}\text{C}$ for 30 min in air. The particles heat treated at

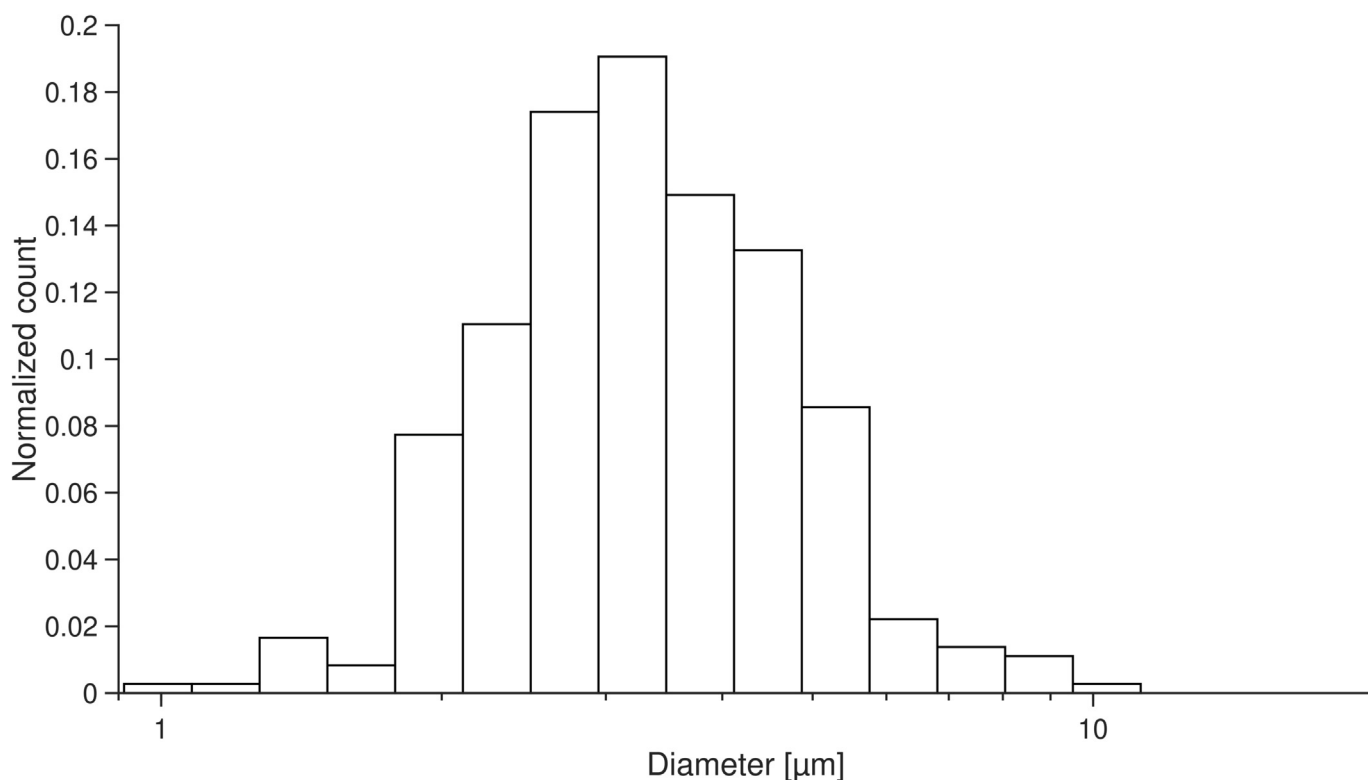


Fig. 7. Size distribution of the spray-dried NMC622 particles produced using final synthesis parameters determined from the particle population ($N > 300$). The geometric mean diameter and the geometric standard deviation were 3.3 μm and 1.44, respectively.

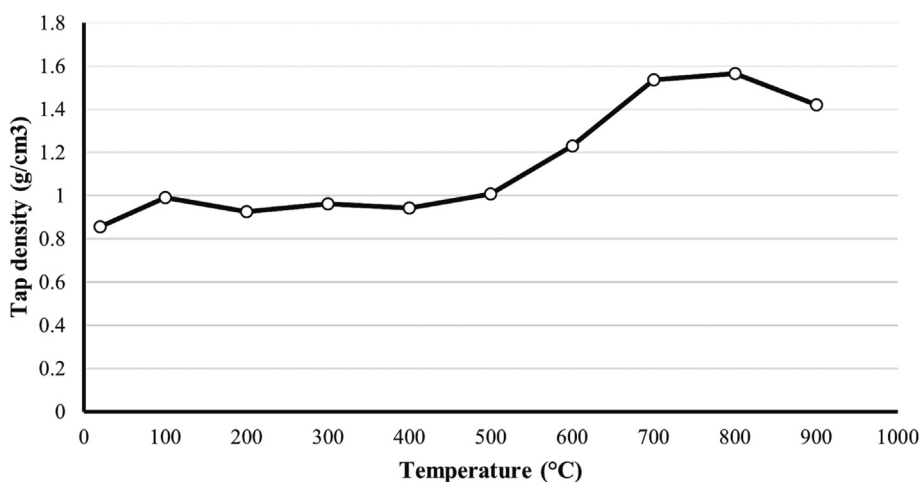


Fig. 8. Tapped density of the NMC622 powder after 30 min heat treatment. The temperature of the heat treatment is shown on x-axis.

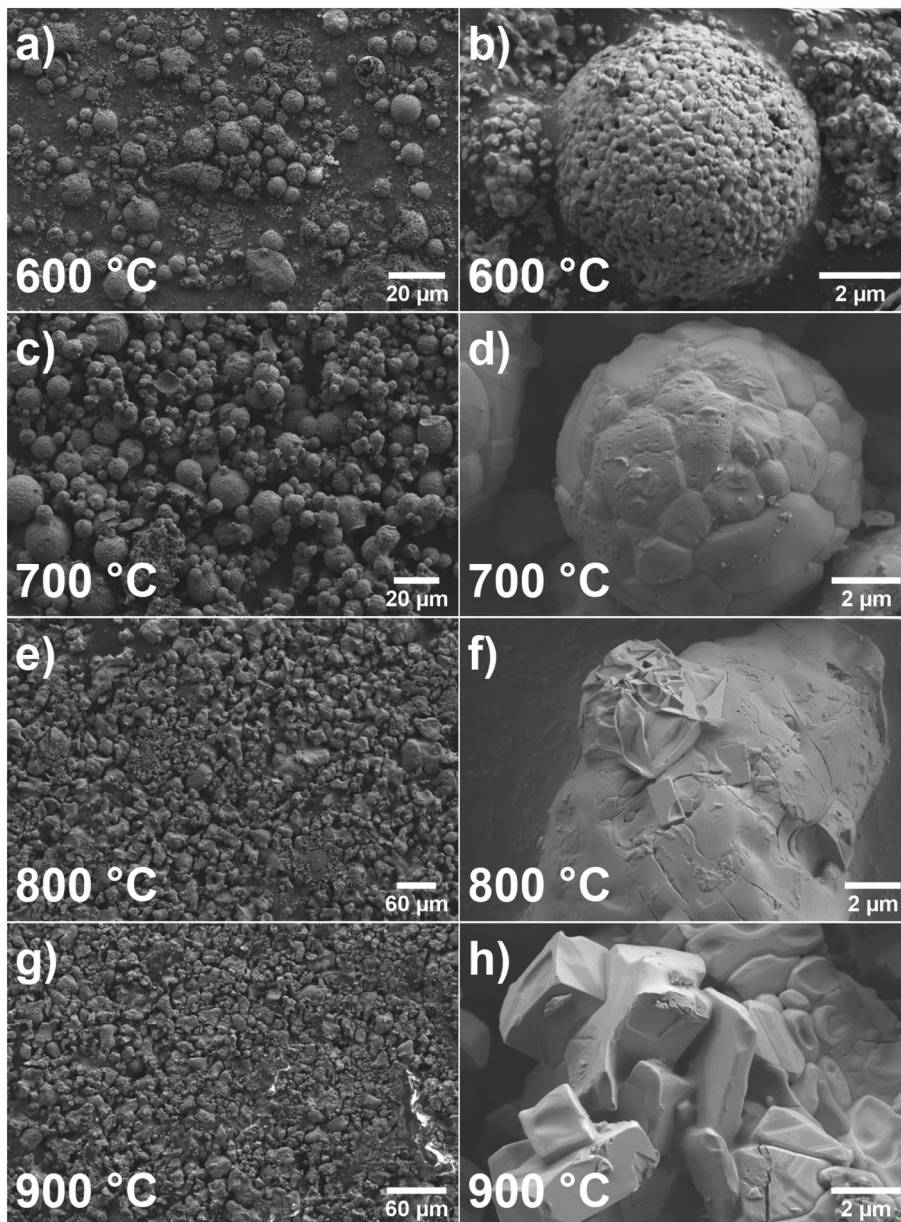


Fig. 9. SEM micrographs of NMC622 sulphate particles heat treated in air at: (a–b) 600 °C, (c–d) 700 °C, (e–f) 800 °C, and (g–h) 900 °C.

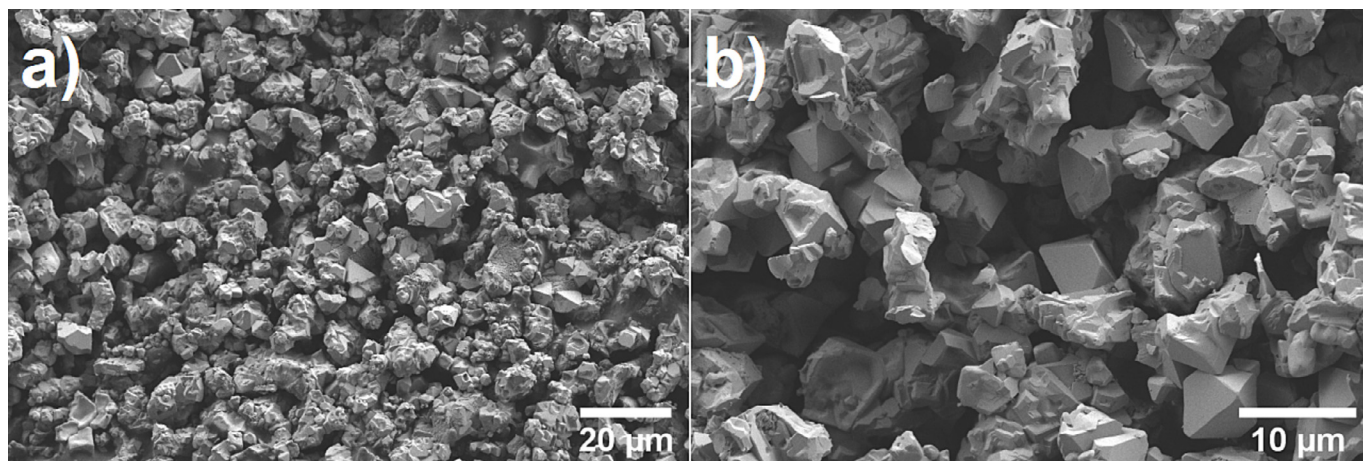


Fig. 10. SEM micrographs of NMC622 heat treated for 16 h in air atmosphere at 850 °C.

600 °C (Fig. 9a) show a spherical shape and appear as single, non-agglomerated particles. As shown in Fig. 9b the particles had a porous surface owing to incomplete sintering, and the primary particles showed only point contact. At 700 °C (Fig. 9c), the particles were still spherical and non-agglomerated. The previously observed incomplete sintering was more complete, i.e., the grains were more fused together, and the grain boundaries closed up, completely removing the porous features. The grain boundaries were difficult to distinguish, and the particles showed almost complete sintering (Fig. 9d). When the particles were heat treated at 800 °C (Fig. 9e) the spherical morphology was lost, and the particles were of irregular geometry. At 900 °C the particles started to assume cubic-like structures with sharp edges, which is likely a result of complete sintering and the formation of large single crystals. It was also noticed visually (see Supplemental Information) that the powder did not melt but rather was sintered at 800 °C and 900 °C, which is contradictory to individual Ni, Mn, and Co sulphate melting points.

Table 2
Molar ratios of Li, Ni, Mn and Co for unwashed and washed NMC622 samples as determined by ICP-OES.

Li precursor		Li:Metal *	Ni:Metal *	Mn:Metal *	Co:Metal *
LiOH	(unwashed)	1.023	0.611	0.190	0.199
	(washed)	0.927	0.610	0.190	0.200
LiCO ₃	(unwashed)	1.077	0.609	0.191	0.200
	(washed)	1.021	0.608	0.192	0.200
LiNO ₃	(unwashed)	1.171	0.611	0.190	0.199
	(washed)	1.097	0.610	0.191	0.200

* Metal refers to the total amount of Li, Ni, Mn and Co.

The most interesting result was that when the particles were heated from 700 °C to 800 °C, the spherical morphology was lost. This result agrees with the TGA results (Fig. 3), tapped density results (Fig. 8), and visual observation of the colour change from light brown to darker brown (see Supplemental Information). These observations support the conclusion that sintering was owing to the simultaneous increase in temperature and sulphate oxidation of NMC622. Also, Lengyel et al. [5] did not observe the morphological changes owing to temperature when already oxidised NMC was heat treated at 900 °C for 2 h.

Fig. 10 shows the NMC622 particles after the complete oxidation of the NMC622 sulphate that was carried out at 850 °C for 3 h and 16 h. The morphological changes of the particles, i.e., sintering and crystallization caused by the release of sulphur, is very similar than observed with the shorter thermal heating times. The results were further confirmed with the ICP-OES analysis that showed a significant decrease of the sulphur content down to

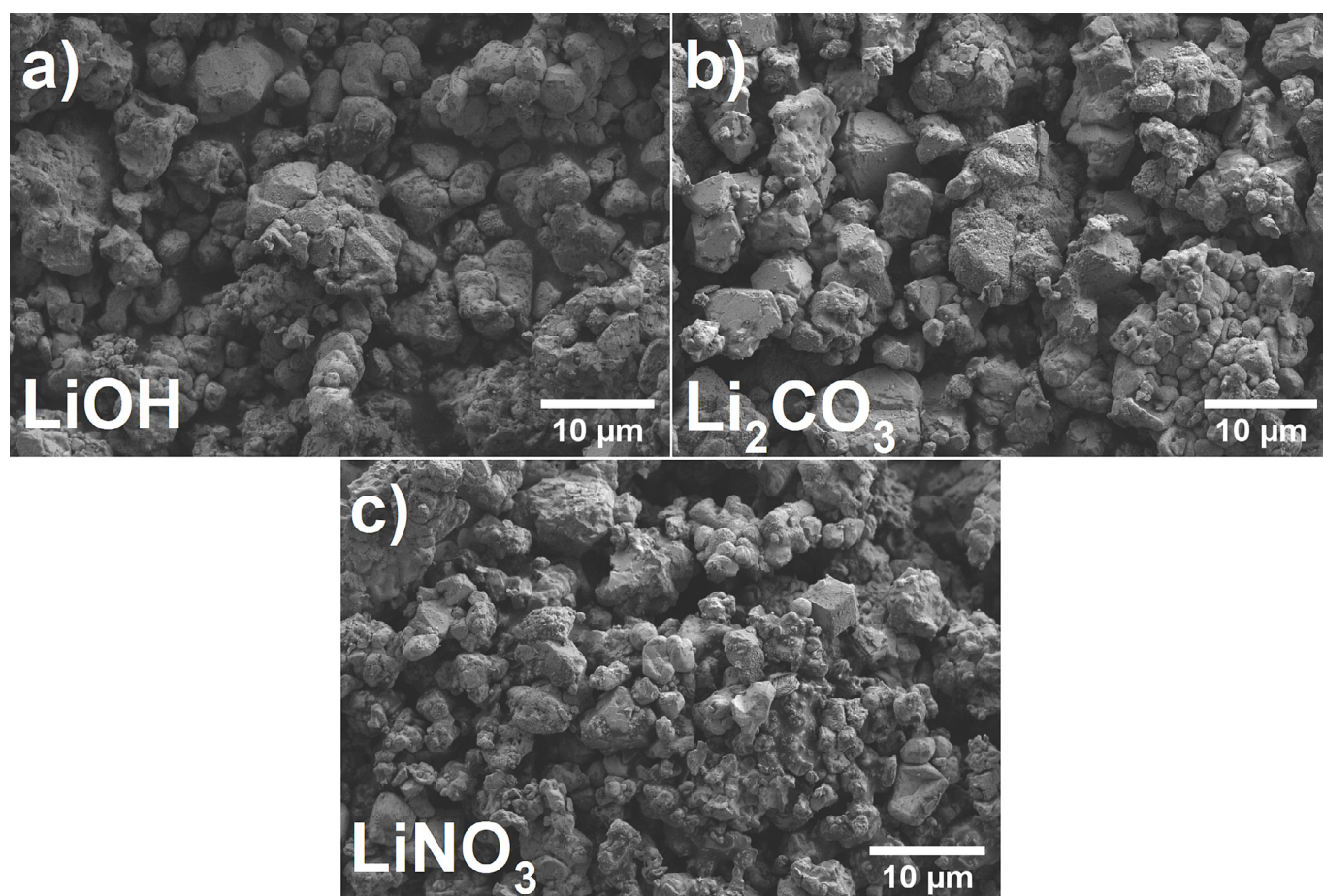


Fig. 11. SEM micrographs of NMC622 after 16 h lithiation at 850 °C with: a) LiOH, b) Li₂CO₃, and c) LiNO₃.

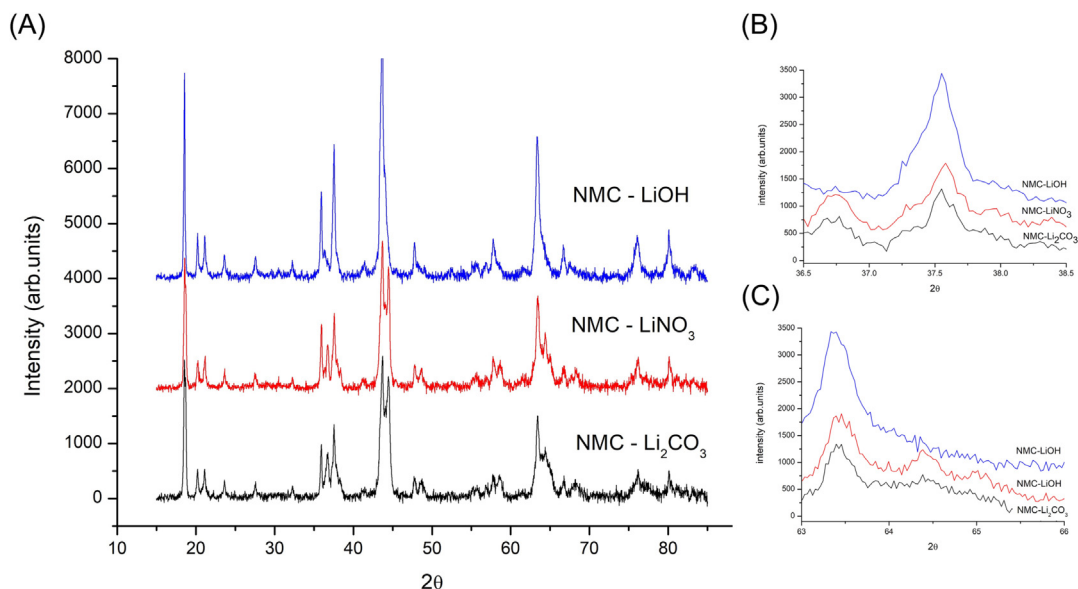


Fig. 12. X-ray diffractograms of NMC622 oxide lithiated with LiOH, LiNO₃, and Li₂CO₃ for 16 h. (The identification of the main peaks is provided in the supplementary Fig. S4.)

1.12 wt% after 3 h and 0.656 wt% after 16 h during the NMC622 sulphate oxidation at 850 °C.

3.5. Lithiation of the oxidized NMC622 particles

3.5.1. Solubility of lithium compounds in NMC622 sulphate–water solution

The solubility of the four solid lithium compounds in the NMC622 sulphate solution was studied as described in Section 2.5. The masses of the Li compounds are listed in Table S2. Li₂SO₄ and LiNO₃ were found to completely dissolve in a given amount of the NMC solution. In contrast, LiOH formed a sediment. Li₂CO₃ is known to have low solubility; therefore, 50 mL of IE water was added to enable complete dissolution. However, this was not sufficient, and sediment was also formed in the NMC + Li₂CO₃ + H₂O solution. The sediment in the NMC + LiOH solution was assumed to be Ni(OH)₂, as evidenced by its green colour (see Supplemental Information Figure S7).

We found that it was not possible to lithiate NMC sulphate solutions in a muffle furnace because the powder melted and adhered to the surfaces of the crucibles when heated to 850 °C. The probable cause of the formation of melted, sticky powders was most likely caused by the release of sulphur from the NMC sulphate solution. The released sulphur formed SO₂, which then reacted with the lithium compounds present in the solution and formed lithium sulphate, which has a melting point of 859 °C. Based on the results, the oxidation of NMC622 sulphate and lithiation were then carried out in two consecutive steps at 850 °C in air atmosphere.

3.5.2. Lithiation of dry NMC622 sulphate particles

The oxidised NMC622 powder was lithiated for 16 h at 850 °C in air atmosphere. The temperature 850 °C was chosen because the results of the TGA studies showed that the lithiation reaction was complete at this temperature for LiOH, LiNO₃, and Li₂CO₃. However, for Li₂SO₄, the lithiation reaction was very slow and incomplete at this temperature, as analysed by ICP-OES and XRD (not shown). Thus, the lithiation results of ICP-OES and XRD are only presented for LiOH and Li₂CO₃.

The lithiation results can be studied by analysing the ratio of lithium to Ni, Mn, and Co metals using ICP-OES. The lithium-to-metal molar ratios for the washed and unwashed NMC622 samples lithiated for 16 h at 850 °C are presented in Table 2. The results show that lithiation is close to unity with all lithium precursors, although it is lower when using LiOH. The table also gives the molar fractions of the Ni, Mn and Co metals. These correspond closely to the expected values for NMC622.

From Fig. 11, we can see that lithiation in a muffle furnace resulted in a morphological change from a spherical shape to a sintered shape.

Fig. 12 shows the XRD data for the NMC622 oxide samples lithiated with LiOH, LiNO₃, and Li₂CO₃. The phases of the final precursor NMC and lithiated NMC particles are typically studied using powder XRD (see Supplemental Information Figures S1–S4). These results show that the main peaks are in good agreement with those of NMC622 reported in the literature [18]. Typically, unlithiated NMC oxide has a Co₃O₄-type spinel phase, and a layered structure is obtained only after lithiation [18,19]. However, some impurity phases are evident in all samples. First, the peaks between 20° and 25° are attributed to the superlattice ordering between NMC-111 and Li₂MnO₃ [5]. Furthermore, peak splitting appears at approximately 37° and 64°. These results indicate the existence of a Li(Ni,Mn)₂O₄ spinel-type phase, as reported by [18] for temperatures above 200 °C. The LiOH-lithiated sample shows slightly higher amounts of the prior but less of the latter impurities.

4. Conclusions

Spray drying is a viable method for synthesising dry, non-hollow NMC622 sulphate particles using aqueous metal sulphate precursors. The physical and chemical phenomena during spray drying were numerically simulated in 1D. The evaporation process was inspected by varying the system parameters of drying air temperature, drying air mass flow rate, and liquid feed mass flow rate. By controlling these parameters, we were able to obtain non-hollow particles, which was a problem in earlier spray drying/pyrolysis studies. The evaporation rate increased with increasing temperature, resulting in lower solid volume percentages of the dried particles. Thus, decreasing the drying air temperature and

the air mass flow-to-liquid mass flow ratio reduced the evaporation rate and increased the solid volume percentage of the produced particles. Using the optimal values for drying air temperature, drying air mass flow rate, and liquid feed mass flow rate obtained from the simulations, we were able to produce non-hollow NMC particles by spray drying. Only approximately 1% of the produced particles were hollow, as observed by SEM analysis and using the ion milling technique to observe the interior of the particles.

The solid NMC622 sulphate particles were then oxidised by heat treatment in a muffle furnace at different temperatures for 30 min. The highest tap density, approximately 1.6 g cm^{-3} , was obtained when the particles were heat treated at 700–800 °C. In this temperature range, the NMC622 sulphate particles began to sinter and lose their spherical morphology. This result agrees with the TGA, tapped density, and visual observations of powder colour. Thus, we can conclude that the morphological change was caused by the oxidation reaction of the sulphate NMC powder when the temperature increased. When we mixed lithium precursors in the NMC sulphate solution before spray drying and then heat treated the spray-dried NMC622 particles, we observed sintering of the particles and powder sticking to the crucible walls in the box furnace when the powder was lithiated at 850 °C. To produce non-hollow solid spherical NMC622 oxide or lithiated NMC particles, a spray pyrolysis reactor should be used after spray drying to prevent contact between individual particles.

The NMC622 oxide powder lithiation was complete at 850 °C, as observed from the lithium-to-metal ratio using ICP-OES, and a pure Li-NMC622 phase was observed by powder XRD when lithium hydroxide was used as the lithium compound.

Declaration of Competing Interest

The authors declare that they have no known competing financial interests or personal relationships that could have appeared to influence the work reported in this paper.

Acknowledgements

The research leading to these results has received funding from Business Finland BatCircle and BatCircle2 projects (5867/31/2018 and 44836/31/2020), Umicore Finland Oy and University of Eastern Finland. We kindly thank Mrs. Virpi Miettinen of SIB Labs for the help during the EM specimen cross-sectioning method development.

Appendix A. Supplementary material

Supplementary data to this article can be found online at <https://doi.org/10.1016/j.appt.2023.104187>.

References

- [1] S. Yang, X. Wang, X. Yang, Z. Liu, Q. Wei, H. Shu, High Tap Density Spherical Li [Ni_{0.5}Mn_{0.3}Co_{0.2}]O₂ Cathode Material Synthesized via Continuous Hydroxide

- Coprecipitation Method for Advanced Lithium-Ion Batteries, *Int. J. Electrochem.* (2012 (2012)), <https://doi.org/10.1155/2012/323560>.
- [2] M. Hietaniemi, T. Hu, J. Välikangas, J. Niittykoski, U. Lassi, Effect of precursor particle size and morphology on lithiation of Ni_{0.6}Mn_{0.2}Co_{0.2}(OH)₂, *J. Appl. Electrochem.* 51 (2021) 1545–1557, <https://doi.org/10.1007/s10800-021-01596-4>.
- [3] W.C. West, J. Soler, M.C. Smart, B.V. Ratnakumar, S. Firdosy, V. Ravi, M.S. Anderson, J. Hrbacek, E.S. Lee, A. Manthiram, Electrochemical behavior of layered solid solution Li₂MnO₃-LiMO₂ (M Ni, Mn, Co) li-ion cathodes with and without alumina coatings, *J. Electrochem. Soc.* 158 (2011) A883–A889, <https://doi.org/10.1149/1.3597319>.
- [4] S. Ahmed, P.A. Nelson, K.G. Gallagher, N. Susrarla, D.W. Dees, Cost and energy demand of producing nickel manganese cobalt cathode material for lithium ion batteries, *J. Power Sources* 342 (2017) 733–740, <https://doi.org/10.1016/j.jpowsour.2016.12.069>.
- [5] M. Lengyel, G. Atlas, D. Elhassid, P.Y. Luo, X. Zhang, I. Belharouak, R.L. Axelbaum, Effects of synthesis conditions on the physical and electrochemical properties of Li_{1.2}Mn_{0.54}Ni_{0.13}Co_{0.13}O₂ prepared by spray pyrolysis, *J. Power Sources* 262 (2014) 286–296, <https://doi.org/10.1016/j.jpowsour.2014.03.113>.
- [6] B. Ebin, M. Doeff, V. Battaglia, Effects of the particle properties on electrochemical performance of nanocrystalline LiAl_{0.1}Cu_{0.1}Mn_{1.8}O₄ cathode materials prepared by ultrasonic spray pyrolysis, *J. Electroanal. Chem.* 792 (2017) 1–7, <https://doi.org/10.1016/j.jelechem.2017.03.031>.
- [7] K. Fröhlich, E. Legotin, F. Bärhold, A. Trifonova, New large-scale production route for synthesis of lithium nickel manganese cobalt oxide, *J. Solid State Electrochem.* 21 (2017) 3403–3410, <https://doi.org/10.1007/s10008-017-3644-x>.
- [8] M. Schiemann, S. Wirtz, V. Scherer, F. Bärhold, Spray roasting of iron chloride FeCl₂: numerical modelling of industrial scale reactors, *Powder Technol.* 245 (2013) 70–79, <https://doi.org/10.1016/j.powtec.2013.04.034>.
- [9] G. Zang, J. Zhang, S. Xu, Y. Xing, Techno-economic analysis of cathode material production using flame-assisted spray pyrolysis, *Energy* 218 (2021), <https://doi.org/10.1016/j.energy.2020.119504>.
- [10] Y. Li, X. Li, Z. Wang, H. Guo, J. Wang, Spray pyrolysis synthesis of nickel-rich layered cathodes LiNi_{1–2x}CoxMnxO₂ (x = 0.075, 0.05, 0.025) for lithium-ion batteries, *J. Energy Chem.* 27 (2018) 447–450, <https://doi.org/10.1016/j.jechem.2017.11.025>.
- [11] S. Jain, D.J. Skamser, T.T. Kodas, Morphology of single-component particles produced by spray pyrolysis, *Aerosol Sci. Tech.* 27 (1997) 575–590, <https://doi.org/10.1080/02786829708965498>.
- [12] M. Lengyel, D. Elhassid, G. Atlas, W.T. Moller, R.L. Axelbaum, Development of a scalable spray pyrolysis process for the production of non-hollow battery materials, *J. Power Sources* 266 (2014) 175–178, <https://doi.org/10.1016/j.jpowsour.2014.04.143>.
- [13] S.H. Ju, Y.C. Kang, The characteristics of Ni–Co–Mn–O precursor and Li(Ni_{1/3}Co_{1/3}Mn_{1/3})O₂ cathode powders prepared by spray pyrolysis, *Ceram. Int.* 35 (2009) 1205–1210, <https://doi.org/10.1016/j.ceramint.2008.06.007>.
- [14] B. Pişkin, C. Savaş Uygur, M.K. Aydınol, Mo doping of layered Li (NixMnyCo_{1–x–y–zMz})O₂ cathode materials for lithium-ion batteries, *Int. J. Energy Res.* 42 (2018) 3888–3898, <https://doi.org/10.1002/er.4121>.
- [15] Y. Zheng, S. Wang, Y. Gao, T. Yang, Q. Zhou, W. Song, C. Zeng, H. Wu, C. Feng, J. Liu, Lithium nickel cobalt manganese oxide recovery via spray pyrolysis directly from the leachate of spent cathode scraps, *ACS Appl. Energy Mater.* 2 (2019) 6952–6959, <https://doi.org/10.1021/acsaem.9b01647>.
- [16] Y. Xiong, T.T. Kodas, Droplet evaporation and solute precipitation during spray pyrolysis, *J. Aerosol Sci* 24 (1993) 893–908, [https://doi.org/10.1016/0021-8502\(93\)90069-L](https://doi.org/10.1016/0021-8502(93)90069-L).
- [17] Y. Ma, M. Svärd, X. Xiao, J.M. Gardner, R.T. Olsson, K. Forsberg, Precipitation and crystallization used in the production of metal salts for Li-Ion battery materials: a review, *Metals*. 10 (2020) 1609, <https://doi.org/10.3390/met10121609>.
- [18] S.-M. Bak, E. Hu, Y. Zhou, X. Yu, S.D. Senanayake, S.-J. Cho, K.-B. Kim, K.Y. Chung, X.-Q. Yang, K.-W. Nam, Structural changes and thermal stability of charged LiNixMnyCozO₂ cathode materials studied by combined in situ time-resolved XRD and mass spectroscopy, *ACS Appl. Mater. Interfaces* 6 (2014) 22594–22601, <https://doi.org/10.1021/am506712c>.
- [19] F. Schipper, E.M. Erickson, C. Erk, J.-Y. Shin, F.F. Chesneau, D. Aurbach, Review—recent advances and remaining challenges for lithium ion battery cathodes, *J. Electrochem. Soc.* 164 (2016) A6220, <https://doi.org/10.1149/2.0351701jes>.